Two-Dimensional Lattice of Out-of-Plane Dinuclear Iron Centers Exhibiting Kondo Resonance

Tao Lin, Guowen Kuang, Weihua Wang, and Nian Lin*

Department of Physics, The Hong Kong University of Science and Technology, Clear Water Bay, Hong Kong

ABSTRACT We present an investigation of two-dimensional coordination networks formed by 5,10,15,20-tetra(4-pyridyl-)porphyrin and iron atoms on a Au(111) surface. The coordination bonds are very robust as evidenced by STM manipulated lateral displacement of an entire network of islands consisting of hundreds of molecules and atoms. We also applied vertical manipulation to detach and attach single Fe atoms at the coordination sites. Moreover, low-temperature tunneling spectroscopy reveals a Kondo resonance at the Fe coordination center. These findings evidence that the network structure is stabilized by a coordination motif in which a pair of vertically aligned Fe atoms is ligated by four equatorial pyridyl groups. Such out-of-plane dinuclear coordination centers provide potential functions, such as catalytic, adsorption, and template for growing three-dimensional framework architectures.

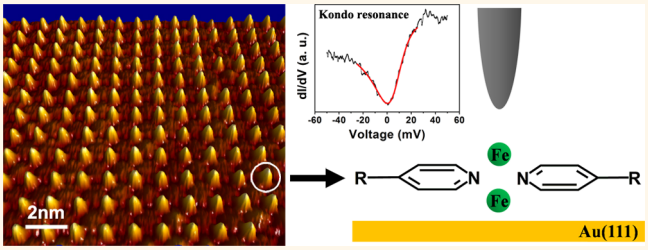

KEYWORDS: dinuclear center · two-dimensional coordination network · scanning tunneling spectroscopy · Kondo resonance · atom manipulation

As a bottom-up approach, surface-assisted supramolecular coordination self-assembly offers a versatile route for designing nanoscale architectures.[1−5] On a surface, coordination usually comprises a single metal atom ligated by organic ligands that lie flat on the surface in a two-fold, three-fold, four-fold,[1−5] or five-fold[6] geometry. The metal centers in these two-dimensional (2D) coordination systems are unsaturated, and their top sites are open for additional ligation.[7] This configuration is expected to possess interesting properties, such as magnetism, catalysis, and gas adsorption.[3,4] For example, Fe centers coordinated by carboxylate ligands on a Cu surface exhibit high-spin magnetic momentum which can be tuned by oxygen adsorption.[8] Dinuclear coordination centers, which are abundant in nature as well as in conventional coordination chemistry in three dimensions, provide rich functions.[9,10] A famous example is dinuclear metal centers in various metalloproteins. This structure plays key roles in respiration or metabolism and thus has attracted intensive attention in biomimetic catalysts.[11] In 2D coordination systems, however, dinuclear coordination centers are very rare. An extensively studied system is the di-M (M = Fe, Co, or Mn) center coordinated by carboxylate or carboxylate/pyridyl ligands, in which two metal atoms are aligned in plane (*i.e.*, parallel to the substrate).[12−21] Interestingly, di-iron centers were found to be much more active than mono-iron ones for O_2 dissociation.[22] The 2D coordination networks containing out-of-plane dinuclear coordination centers in which two metal atoms align perpendicular to the network plane are highly interesting because the outstanding metal atoms may be extremely reactive as they are more open for on-top binding. Furthermore, these atoms provide sites for axial ligation which may extend the 2D networks into three-dimensional (3D) frameworks. To date, however, such out-of-plane dinuclear coordination systems are not reported.

Here we report on a study of surface-assisted self-assembly of 5,10,15,20-tetra-(4-pyridyl)porphyrin (TPyP, as shown in Figure 1a) and Fe on a Au(111) surface. In solution phase, TPyP forms 3D coordination

* Address correspondence to phnlin@ust.hk.

Received for review May 21, 2014 and accepted July 31, 2014.

Published online August 01, 2014
10.1021/nn502765g

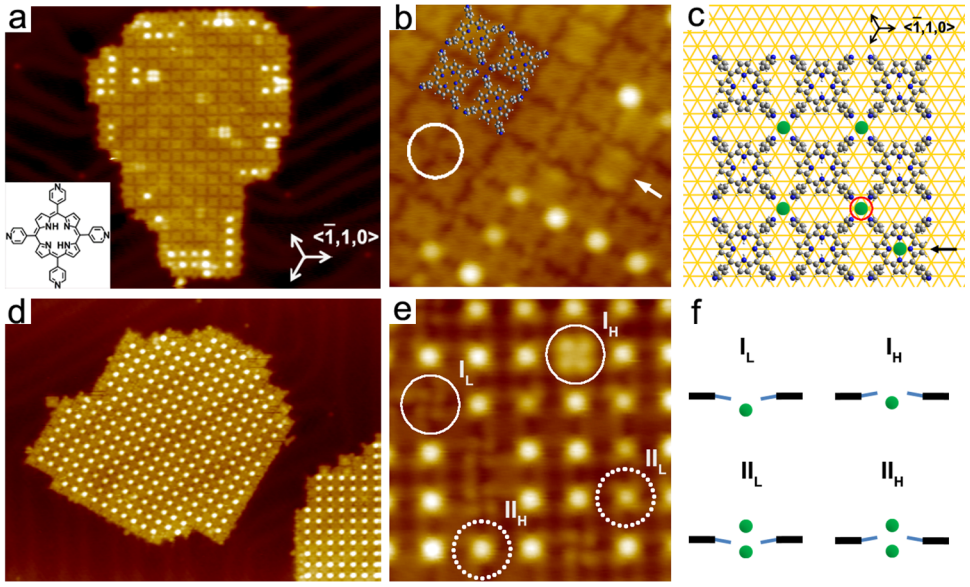

Figure 1. (a) STM image (40 × 30 nm^2) of a network island formed out of TPyP and low-dosage Fe. Inset: Chemical structure of TPyP. (b) High-resolution STM image (8.9 × 8.9 nm^2) showing metalated FeTPyP molecules (indicated by the white arrow) and the cloverleaf junctions (in the white circle). (c) Tentative model of the network structure (green dots, Fe atoms). The black arrow indicates a metalated FeTPyP molecule, and the red circle highlights a type-II junction. (d) STM image (40 × 30 nm^2) showing two network islands formed out of TPyP and high-dosage Fe. (e) High-resolution STM image (8.3 × 8.3 nm^2) showing four types of junctions. (f) Tentative model of the four types of junctions (green dot, Fe atom; blue line, pyridyl group; black rectangle, porphyrin core).

frameworks with Mn, Fe, Ag, Co, Zn, or Cu.[23−28] On the surface, TPyP can coordinate with Au or Cu, forming 2D Kagome or square networks.[29−31] In this study, we found that TPyP and Fe form extended 2D networks exhibiting a nearly square lattice. Surprisingly, the network islands that consist of hundreds of molecules and atoms could be moved laterally on the surface by a scanning tunneling microscope (STM) tip without disruption. STM has been used to manipulate individual atoms,[32,33] molecules,[34,35] supramolecular clusters,[36−38] and supramolecular chains.[39,40] Manipulation of such large size supramolecular structures has not been achieved because the intermolecule binding force is normally weaker than the diffusion energy barrier when the structures become large. Our results clearly demonstrate that the cohesive energy of the coordination bonds in the networks is very high. We also conducted vertical manipulation at coordination junctions to "pick-up" or "put-down" single Fe atoms reversibly. Furthermore, we used scanning tunneling spectroscopy (STS) to resolve Kondo resonance at the coordination junctions before and after the vertical manipulation. On the basis of these findings, we conclude that the 2D FeTPyP coordination networks are stabilized by a novel dinuclear coordination motif in which two Fe atoms are aligned vertically to the network plane and ligated to four equatorial pyridyl ligands.[41,42]

RESULTS AND DISCUSSION

On Au(111), TPyP molecules form a close-packed monolayer that is stabilized by weak intermolecule interactions similar to that on Ag(111).[43] After dosing small amounts of Fe and followed by a thermal annealing treatment at 150 °C, networks showing nearly square lattice emerged (see Figure 1a). The high-symmetric direction of the networks follows $\langle\bar{1}10\rangle$ or equivalent directions of the Au(111) surface lattice. The lattice constant of the network phase along $\langle\bar{1}10\rangle$ is 1.43 ± 0.02 nm, which is five times the lattice constant (0.288 nm) of the Au(111) substrate. Along the orthogonal direction, which follows $\langle11\bar{2}\rangle$ direction of Au(111), the network lattice constant is 1.49 ± 0.03 nm, which is three times the periodic distance of 0.498 nm of the Au(111) substrate along the $\langle11\bar{2}\rangle$ direction. Figure 1b is a high-resolution image of the network structure. One can see that TPyP molecules show two types of intramolecular appearance: one type exhibits a dark depression at the center, and the other type (marked by an arrow) shows two protrusions at two opposite edges. We attribute the first type as free base TPyP and the second type as Fe-metalated FeTPyP since before Fe deposition we only observed the first type.[31,43,44] Fe metalation is further confirmed by Kondo resonance (see later discussion). Detailed inspection reveals that both types of molecules have a slightly longer axis (*i.e.*, showing C_{2v} symmetry), which arises from saddle-shaped molecular conformation.[45] At the four corners of each molecule, there are "finger-like" features that can be assigned to pyridyl (py) functional groups. At the junction of four adjacent molecules, four py groups point inwardly, forming a cloverleaf; see the circle in Figure 1b. Such configuration strongly hints that the four py groups bind to a

central agent, presumably an Fe atom (or ion) *via* coordination bonds. The metal centers in the surface coordination systems are often not resolved by STM due to either deficient electronic states or lower geometrical height.[46] The existence of Fe at the cloverleaf junctions is confirmed by Kondo resonance (see later discussion). Figure 1c shows a structural model based on the STM data (note that the orientation of the pyridyl ligands may take a different angle). The neighboring TPyP molecules are linked *via* four-fold Fe-py coordination in which Fe−N bond length is 0.25 nm if it is assumed that Fe and N atoms are in the same plane. This value falls in the range of typical metal−organic coordination bond length.[1]

In Figure 1a,b, bright dots appear at some junctions in the network. In the following discussion, we denote the cloverleaf junctions as type-I and the junctions with dots as type-II. Both types occupy identical sites in the network lattice. The circle in Figure 1c highlights the position of a type-II junction. The population of the type-II junctions increases at higher Fe dosage. Figure 1d shows two network islands formed on a sample with high Fe dosage. One can see that the lattice and orientation of these networks are identical to those of the networks formed with the low Fe dosage sample. The major difference is that the junction sites are almost fully occupied by bright dots, namely, type-II junctions. The high-resolution data reveal that the molecules in the network are exclusively metalated by Fe (confirmed by Kondo resonance). High-dosage Fe thus resulted in two effects: metalation of the porphyrin cores and generation of type-II junctions. Since a type-I junction already contains an Fe atom, we propose that the bright dot in the type-II junction accounts for a two-Fe junction, in which an Fe atom sits on top of a type-I junction. The bonding between the two Fe atoms in the junction is not fully understood. Nevertheless, we speculate that the top Fe binds with the py groups as we will demonstrate later that type-II junctions remarkably enhance the cohesive energy of the network lattice. Moreover, Figure 1b shows that the type-II dots may appear in two heights, as highlighted by the dotted circles in Figure 1e and denoted as II_L and II_H for the low and high ones, respectively. We also observed that type-I junctions also have two different appearances, as highlighted by the solid circles in Figure 1e. In Figure 1e, there are four types of junctions: normal type-I junction (I_L), bright type-I junction (I_H), low type-II (II_L), and high type-II (II_H). It is known that the phenyl groups attached to a porphyrin core may be bent downwardly or upwardly with respect to the porphyrin core;[47] we suggest that the different appearances of I_L and I_H or II_L and II_H can be ascribed to the same effect; that is, the pyridyl groups are bent downwardly or upwardly for $I_L(II_L)$ or $I_H(II_H)$, respectively. Tentative side-view models of the four types of junctions are plotted in Figure 1f.

We conducted lateral manipulation to examine the bond strength of the networks. The manipulation consists of three steps: (1) vertical approach of the STM tip 0.3−0.4 nm toward the edge of a network island, (2) lateral displacement of the STM tip, and (3) retraction of the STM tip. Figure 2a,b shows an example of lateral manipulation of an island consisting of about 330 molecules that are linked predominantly by type-II junctions. The red arrow in Figure 2a indicates the tip displacement path. Figure 2b shows that the island has been shifted by 2.8 nm, taking the top right corner as a reference (the dashed frame marks the island periphery before the manipulation). The internal features of the islands including a vacancy and several type-I junctions remain unchanged after the manipulation. We found that when a network island is attached to a step edge, it could not be displaced using the same protocol, presumably due to the interactions between the island and the step. It is quite surprising that large supramolecular structures containing hundreds of molecules can be moved without losing their integrity. Apparently, the cohesive energy of the coordination bonds is larger than the diffusion energy barrier of the entire islands. Considering the size of the islands, the strength of the coordination bonds is remarkable.

To compare the bond strength of type-I and type-II junctions, we manipulated an island shown in Figure 2c, which contains many type-I junctions. Particularly, there exists a chain of type-I junctions in this island as indicated by the white arrow. We conducted multiple manipulations at this island. Figure 2d shows that the first manipulation (indicated by the red arrow in Figure 2c) broke the island into two parts along the type-I junction chain. The two parts are connected by a single type-II junction. Figure 2e shows that another manipulation (indicated by the blue arrow in Figure 2d) tore the two parts further apart, while the type-II junction linking the two parts still remained. Apparently, type-II junctions are much stronger than type-I. In other words, the two-Fe junction substantially enhances the cohesive energy of the coordination bond. We propose that the top Fe also bonds to the py groups, hence strengthening intermolecular binding. Another likely reason for lateral manipulation of the networks containing type-II junctions is that, when a second Fe atom binds to the lower Fe atom, the bonding of the lower Fe atom with the Au substrate is weakened. Such effects have previously been shown.[48] As a result of the weakened adsorbate−substrate bonds, the barriers for lateral movements are reduced.

We also conducted vertical manipulation at the junctions to detach and attach single Fe atoms: First, the STM tip was positioned on top of a II_H junction, for example, the one circled in Figure 3a. Then a bias voltage of −2 V was applied. At this condition, the top Fe atom could be transferred to the tip and the II_H

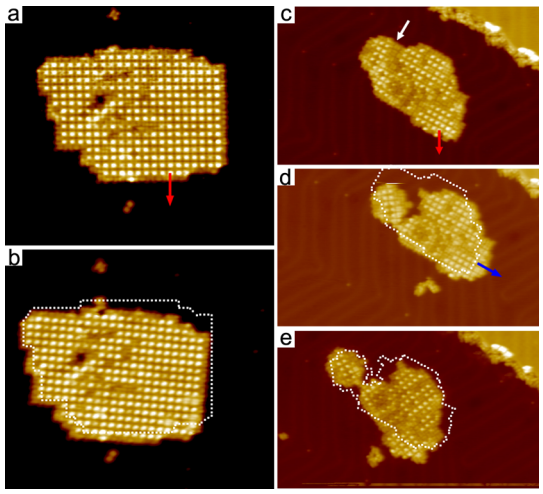

Figure 2. Lateral manipulation of FeTPyP islands. (a,b) Lateral manipulation of an island containing about 330 TPyP molecules. The red arrow in (a) marked the tip path for manipulation (image size: 40 × 35.5 nm^2). (c−e) Lateral manipulation of an island containing a type-I junction line as indicated by the white arrow in (c). The red arrow in (c) and the blue arrow in (d) show two tip paths for manipulations (image size: 50 × 30 nm^2).

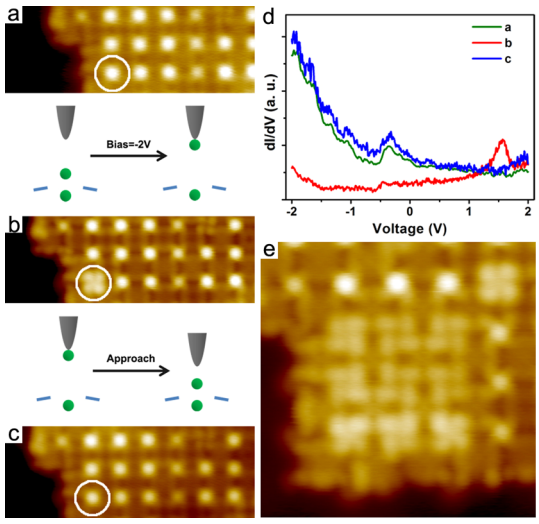

Figure 3. Vertical manipulation of type-II junctions: (a,b) II$_H$ to I$_H$; (b,c) I$_H$ to II$_H$ (image size: 12.5 × 4.3 nm^2). (d) d*I*/d*V* spectra of clean Au(111) acquired using the tip in (a−c). (e) A 3 × 3 I$_H$ structure fabricated by multiple vertical manipulations (image size: 7.7 × 7.7 nm^2).

junction was changed to a I$_H$ junction, as shown in Figure 3b. Note that attachment of the Fe atom at the tip end improved STM resolution as manifested by Figure 3b. We acquired tunneling spectra on a clean Au surface area to examine the state of the tip before and after the vertical manipulation. The green curve in Figure 3d is a d*I*/d*V* spectrum acquired using a clean tip before the manipulation, showing the surface-state onset of the Au(111) at −0.45 V. After the manipulation, the surface-state onset becomes weaker and a peak emerges at 1.55 V (the red curve in Figure 3d). This new state can be attributed to the attachment of a single atom at the tip end. The attached Fe atom could be transferred back to a I$_H$ junction by approaching the tip 0.3 nm toward the junction. Figure 3c shows that the I$_H$ junction regained the Fe atom and was changed back to a II$_H$ junction. Meanwhile, the STM resolution changed to the previous state (cf. Figure 3a), and the 1.55 V peak in the d*I*/d*V* spectrum disappears (cf. the blue curve in Figure 3d), indicating that the tip lost the Fe atom and recovered its initial state. Dozens of vertical manipulations were successfully performed following this protocol. Figure 3e shows an example in which a 3 × 3 matrix of I$_H$ junctions was fabricated by repeatedly picking up Fe atoms one by one from the II$_H$ junctions.

The network provides an interesting system to study magnetic characteristics of the coordinated Fe species. When adsorbed on a metallic surface, spin of a magnetic impurity is screened by surface electrons, giving rise to Kondo effect. Kondo effect can be detected by means of tunneling spectroscopy. We acquired tunneling spectra at the four types of junctions as well as at the central Fe of FeTPyP molecules. Figure 4a shows, from top to bottom, the d*I*/d*V* spectra measured at the center of a FeTPyP, at II$_H$, II$_L$, I$_H$, and I$_L$ junctions (the signals of I$_H$ and I$_L$ are multiplied by a factor of 10). All of these curves exhibit a dip-like line shape that can be fitted using a Fano function[49]

$$f(x) = A \times \frac{[q+(x-\epsilon_0)/\Gamma]^2}{1+[(x-\epsilon_0)/\Gamma]^2} + B$$

Variable-temperature measurements show that temperature-dependent evolution of the line shape agrees with the expected Kondo characteristics at elevated temperatures. So we confirm that the observed dip-like line shape is a Kondo resonance. Kondo resonance probed by STM has been reported in single magnetic atoms,[50−52] organic radicals,[53,54] metal−porphyrin, and organic−metal complexes.[55−61] Our findings represent the first observation of Kondo resonance of magnetic metal centers in a metal−organic coordination network system.

Fano fitting of the Kondo resonances yields Γ values of 12.8 ± 0.4, 9.8 ± 0.7, 12.3 ± 1.2, 15.5 ± 3.0, and 11.8 ± 2.6 mV for FeTPyP, II$_H$, II$_L$, I$_H$, and I$_L$, respectively. We found that the Kondo resonance can be detected at the type-I junctions and the Fe center in FeTPyP independent of tip-to-sample distance; however, the Kondo resonance of the type-II junctions appeared only when the tip was brought sufficiently close to the junction. Figure 4b (left panel) displays tunneling current as a function of tip height measured as the tip was vertically approaching a II$_H$ junction in the tunneling regime. As the tip is moved down by 2.0 Å, d(LnI)/d*z* changes. Figure 4b (right panel) displays the d*I*/d*V* spectra measured at different tip heights. The Kondo resonance emerges only when the tip displacement is greater than 1.8 Å, that is, at the same tip−sample distance when d(LnI)/d*z* changes. It was reported that as tip−sample distance varies from tunneling regime

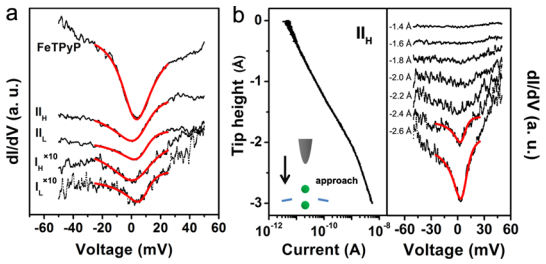

Figure 4. Kondo resonance of Fe centers. (a) d*I*/d*V* spectra (top to bottom) measured at the center of a FeTPyP, at II_H, II_L, I_H, and I_L junctions, respectively. Red curves are the fitting curves using Fano function (the curves of I_H and I_L are multiplied by 10). (b) Left panel: *I*–*z* curve measured on top of a II_H junction. Right panel: d*I*/d*V* spectra measured at the II_H junction at different tip heights. Red curves are the fitting curves using the Fano function.

to contact regime, Kondo temperature may undergo a change, but the Kondo resonance is present in all distances.[62–65] In our system, within the tunneling regime, the Kondo resonance at the type-II junctions is on or off at short or long tip–sample distances, respectively. One possible mechanism is that, at a shorter tip–sample distance, the top Fe atom in the junction may be pushed into closer contact with the screening electrons, which is signified by d(LnI)/d*z* change. In this new configuration, the coupling between the top Fe and the screening electrons is enhanced, thus the Kondo feature is magnified. For the type-I junctions and the FeTPyP, the coupling between the Fe centers and the screening electrons is not changed by the tip height, so the Kondo resonance is independent of tip-to-sample distance.

CONCLUSION

In summary, we have investigated surface-assisted coordination self-assembly of TPyP molecules and Fe atoms on Au(111). On the basis of STM lateral and vertical manipulation experiments and Kondo spectroscopy measurements, we discovered that the Fe-metalated porphyrin molecules are linked through an out-of-plane dinuclear Fe coordination motif in which two vertically aligned Fe atoms are coordinated by four equatorial pyridyl ligands. This structure consists of regularly ordered Fe atoms that are in two well-defined states, namely, single Fe atoms coordinated in porphyrin cores and Fe pairs ligated to pyridyl groups. These distinctive Fe species might provide interesting magnetic, catalytic, or gas adsorption properties. Last but not least, we would like to point out that this novel dinuclear coordination motif deserves further studies using advanced spectroscopy and state-of-the-art simulations to elucidate its binding configuration including Fe–N bond length, pyridyl conformation, the Fe atoms' height, and Fe–Fe bond length, *etc.*

METHODS

Experiments were performed in an ultrahigh vacuum system (Omicron Nanotechnology) with base pressure below 5×10^{-10} mbar. A single-crystalline Au(111) substrate was cleaned by argon-ion sputtering and annealing to ~630 °C. The TPyP molecule was thermally evaporated by a molecular beam evaporator and deposited onto the Au(111) substrate which was held at room temperature. The evaporation temperatures for TPyP molecule were 380 °C. The STM measurements were performed at 4.9 K, and the STM imaging parameters were $U = 1.00$ V and $I = 0.30$ nA.

Conflict of Interest: The authors declare no competing financial interest.

Acknowledgment. This work was supported by Hong Kong RGC 602712.

REFERENCES AND NOTES

1. Barth, J. V. Molecular Architectonic on Metal Surfaces. *Annu. Rev. Phys. Chem.* **2007**, *58*, 375–407.
2. Stepanow, S.; Lin, N.; Barth, J. V. Modular Assembly of Low-Dimensional Coordination Architectures on Metal Surfaces. *J. Phys.: Condens. Matter* **2008**, *20*, 184002.
3. Lin, N.; Stepanow, S.; Ruben, M.; Barth, J. V. Surface-Confined Supramolecular Coordination Chemistry. *Top. Curr. Chem.* **2009**, *287*, 1–44.
4. Barth, J. V. Fresh Perspectives for Surface Coordination Chemistry. *Surf. Sci.* **2009**, *603*, 1533–1541.
5. Bartels, L. Tailoring Molecular Layers at Metal Surfaces. *Nat. Chem.* **2010**, *2*, 87–95.
6. Écija, D.; Urgel, J. I.; Papageorgiou, A. C.; Joshi, S.; Auwärter, W.; Seitsonen, A. P.; Klyatskaya, S.; Ruben, M.; Fischer, S.; Vijayaraghavan, S.; *et al.* Five-Vertex Archimedean Surface Tessellation by Lanthanide-Directed Molecular Self-Assembly. *Proc. Natl. Acad. Sci. U.S.A.* **2013**, *110*, 6678–6681.
7. Burwell, R.; Taylor, K.; Haller, G. Texture of Chromium Oxide Catalysts. *J. Phys. Chem.* **1967**, *71*, 4580–4581.
8. Gambardella, P.; Stepanow, S.; Dmitriev, A.; Honolka, J.; De Groot, F. M. F.; Lingenfelder, M.; Sen Gupta, S.; Sarma, D. D.; Bencok, P.; Stanescu, S.; *et al.* Supramolecular Control of the Magnetic Anisotropy in Two-Dimensional High-Spin Fe Arrays at a Metal Interface. *Nat. Mater.* **2009**, *8*, 189–193.
9. Chakrabarty, R.; Mukherjee, P. S.; Stang, P. J. Supramolecular Coordination: Self-Assembly of Finite Two- and Three-Dimensional Ensembles. *Chem. Rev.* **2011**, *111*, 6810–6918.
10. Cook, T. R.; Zheng, Y. R.; Stang, P. J. Metal–Organic Frameworks and Self-Assembled Supramolecular Coordination Complexes: Comparing and Contrasting the Design, Synthesis, and Functionality of Metal–Organic Materials. *Chem. Rev.* **2013**, *113*, 734–777.
11. Lippard, S. J. The Inorganic Side of Chemical Biology. *Nat. Chem. Biol.* **2006**, *2*, 504–507.
12. Dmitriev, A.; Spillmann, H.; Lin, N.; Barth, J. V.; Kern, K. Modular Assembly of Two-Dimensional Metal–Organic Coordination Networks at a Metal Surface. *Angew. Chem., Int. Ed.* **2003**, *42*, 2670–2673.
13. Stepanow, S.; Lingenfelder, M.; Dmitriev, A.; Spillmann, H.; Delvigne, E.; Lin, N.; Deng, X.; Cai, C.; Barth, J. V.; Kern, K. Steering Molecular Organization and Host–Guest Interactions Using Two-Dimensional Nanoporous Coordination Systems. *Nat. Mater.* **2004**, *3*, 229–233.
14. Lingenfelder, M. A.; Spillmann, H.; Dmitriev, A.; Stepanow, S.; Lin, N.; Barth, J. V.; Kern, K. Towards Surface-Supported Supramolecular Architectures: Tailored Coordination Assembly of 1,4-Benzenedicarboxylate and Fe on Cu(100). *Chem.—Eur. J.* **2004**, *10*, 1913–1919.
15. Lin, N.; Stepanow, S.; Vidal, F.; Barth, J. V.; Kern, K. Manipulating 2D Metal-Organic Networks *via* Ligand Control. *Chem. Commun.* **2005**, 1681–1683.

16. Seitsonen, A. P.; Lingenfelder, M.; Spillmann, H.; Dmitriev, A.; Stepanow, S.; Lin, N.; Kern, K.; Barth, J. V. Density Functional Theory Analysis of Carboxylate-Bridged Diiron Units in Two-Dimensional Metal−Organic Grids. *J. Am. Chem. Soc.* **2006**, *128*, 5634–5635.
17. Stepanow, S.; Lin, N.; Barth, J. V.; Kern, K. Surface-Template Assembly of Two-Dimensional Metal−Organic Coordination Networks. *J. Phys. Chem. B* **2006**, *110*, 23472–23477.
18. Clair, S.; Pons, S.; Fabris, S.; Baroni, S.; Brune, H.; Kern, K.; Barth, J. V. Monitoring Two-Dimensional Coordination Reactions: Directed Assembly of Co-Terephthalate Nanosystems on Au(111). *J. Phys. Chem. B* **2006**, *110*, 5627–5632.
19. Zhang, Y.-F.; Zhu, N.; Komeda, T. Mn-Coordinated Stillbenedicarboxylic Ligand Supramolecule Regulated by the Herringbone Reconstruction of Au(111). *J. Phys. Chem. C* **2007**, *111*, 16946–16950.
20. Langner, A.; Tait, S. L.; Lin, N.; Rajadurai, C.; Ruben, M.; Kern, K. Self-Recognition and Self-Selection in Multicomponent Supramolecular Coordination Networks on Surfaces. *Proc. Natl. Acad. Sci. U.S.A.* **2007**, *104*, 17927–17930.
21. Tait, S. L.; Wang, Y.; Costantini, G.; Lin, N.; Baraldi, A.; Esch, F.; Petaccia, L.; Lizzit, S.; Kern, K. Metal−Organic Coordination Interactions in Fe-Terephthalic Acid Networks on Cu(100). *J. Am. Chem. Soc.* **2008**, *130*, 2108–2113.
22. Fabris, S.; Stepanow, S.; Lin, N.; Gambardella, P.; Dmitriev, A.; Honolka, J.; Baroni, S.; Kern, K. Oxygen Dissociation by Concerted Action of Di-iron Centers in Metal−Organic Coordination Networks at Surfaces: Modeling Non-Heme Iron Enzymes. *Nano Lett.* **2011**, *11*, 5414–5420.
23. Kumar, R. K.; Goldberg, I. Supramolecular Assembly of Heterogeneous Multiporphyrin Arrays: Structures of $[\{Zn^{II}(tpp)\}_2(tpyp)]$ and the Coordination Polymer $[\{[Mn^{III}(tpp)]_2(tpyp)(ClO_4)_2\}_\infty]$. *Angew. Chem., Int. Ed.* **1998**, *37*, 3027–3030.
24. Hagrman, D.; Hagrman, P. J.; Zubieta, J. Solid-State Coordination Chemistry: The Self-Assembly of Microporous Organic−Inorganic Hybrid Frameworks Constructed from Tetrapyridylporphyrin and Bimetallic Oxide Chains or Oxide Clusters. *Angew. Chem., Int. Ed.* **1999**, *38*, 3165–3168.
25. Carlucci, L.; Ciani, G.; Proserpio, D. M.; Porta, F. Open Network Architectures from the Self-Assembly of $AgNO_3$ and 5,10,15,20-Tetra(4-pyridyl)porphyrin (H_2tpyp) Building Blocks: The Exceptional Self-Penetrating Topology of the 3D Network of $[Ag_8(Zn^{II}tpyp)_7(H_2O)_2](NO_3)_8$. *Angew. Chem., Int. Ed.* **2003**, *42*, 317–322.
26. Pan, L.; Huang, X.; Phan, H.-L. N.; Emge, T. J.; Li, J.; Wang, X. 1-D Infinite Array of Metalloporphyrin Cages. *Inorg. Chem.* **2004**, *43*, 6878–6880.
27. Carlucci, L.; Ciani, G.; Proserpio, D. M.; Porta, F. Four New 2D Porous Polymeric Frames from the Self-Assembly of Silver Triflate and Silver Tosylate with Free-Base and Zn-Metallated 5,10,15,20-Tetra(4-pyridyl)porphyrin. *CrystEngComm* **2005**, *7*, 78–86.
28. Ohmura, T.; Usuki, A.; Fukumori, K.; Ohta, T.; Ito, M.; Tatsumi, K. New Porphyrin-Based Metal−Organic Framework with High Porosity: 2-D Infinite 22.2-Å Square-Grid Coordination Network. *Inorg. Chem.* **2006**, *45*, 7988–7990.
29. Shi, Z. L.; Lin, N. Porphyrin-Based Two-Dimensional Coordination Kagome Lattice Self-Assembled on a Au(111) Surface. *J. Am. Chem. Soc.* **2009**, *131*, 5376–5377.
30. Shi, Z.; Lin, N. Self-Assembly of a Two-Dimensional Bimetallic Coordination Framework and Dynamic Control of Reversible Conversions to Homo-Metallic Hydrogen-Bond Arrays. *ChemPhysChem* **2010**, *11*, 97–100.
31. Li, Y.; Xiao, J.; Shubina, T. E.; Chen, M.; Shi, Z.; Schmid, M.; Steinrück, H.-P.; Gottfried, J. M.; Lin, N. Coordination and Metalation Bifunctionality of Cu with 5,10,15,20-Tetra(4-pyridyl)porphyrin: Toward a Mixed-Valence Two-Dimensional Coordination Network. *J. Am. Chem. Soc.* **2012**, *134*, 6401–6408.
32. Eigler, D. M.; Schweizer, E. K. Positioning Single Atoms with a Scanning Tunneling Microscope. *Nature* **1990**, *344*, 524–526.
33. Crommie, M. F.; Lutz, C. P.; Eigler, D. M. Confinement of Electrons to Quantum Corrals on a Metal-Surface. *Science* **1993**, *262*, 218–220.
34. Mielke, J.; Selvanathan, S.; Peters, M.; Schwarz, J.; Hecht, S.; Grill, L. Molecules with Multiple Switching Units on a Au(111) Surface: Self-Organization and Single-Molecule Manipulation. *J. Phys.: Condens. Matter* **2012**, *24*, 394013.
35. Kudernac, T.; Ruangsupapichat, N.; Parschau, M.; Maciá, B.; Katsonis, N.; Harutyunyan, S. R.; Ernst, K.-H.; Feringa, B. L. Electrically Driven Directional Motion of a Four-Wheeled Molecule on a Metal Surface. *Nature* **2011**, *479*, 208–211.
36. Böhringer, M.; Morgenstern, K.; Schneider, W. D.; Berndt, R. Separation of a Racemic Mixture of Two-Dimensional Molecular Clusters by Scanning Tunneling Microscopy. *Angew. Chem., Int. Ed.* **1999**, *38*, 821–823.
37. Nickel, A.; Ohmann, R.; Meyer, J.; Grisolia, M.; Joachim, C.; Moresco, F.; Cuniberti, G. Moving Nanostructures: Pulse-Induced Positioning of Supramolecular Assemblies. *ACS Nano* **2013**, *7*, 191–197.
38. Urgel, J. I.; Ecija, D.; Auwärter, W.; Barth, J. V. Controlled Manipulation of Gadolinium-Coordinated Supramolecules by Low-Temperature Scanning Tunneling Microscopy. *Nano Lett.* **2014**, *14*, 1369–1373.
39. Marschall, M.; Reichert, J.; Weber-Bargioni, A.; Seufert, K.; Auwärter, W.; Klyatskaya, S.; Zoppellaro, G.; Ruben, M.; Barth, J. V. Random Two-Dimensional String Networks Based on Divergent Coordination Assembly. *Nat. Chem.* **2010**, *2*, 131–137.
40. Heim, D.; Écija, D.; Seutert, K.; Auwärter, W.; Aurisicchio, C.; Fabbro, C.; Bonifazi, D.; Barth, J. V. Self-Assembly of Flexible One-Dimensional Coordination Polymers on Metal Surfaces. *J. Am. Chem. Soc.* **2010**, *132*, 6783–6790.
41. Xiao, R.; Fritsch, D.; Kuz'min, M. D.; Koepernik, K.; Eschrig, H.; Richter, M.; Vietze, K.; Seifert, G. Co Dimers on Hexagonal Carbon Rings Proposed as Subnanometer Magnetic Storage Bits. *Phys. Rev. Lett.* **2009**, *103*, 187201.
42. Krenner, W.; Klappenberger, F.; Kühne, D.; Diller, K.; Qu, Z.-R.; Ruben, M.; Barth, J. V. Positioning of Single Co Atoms Steered by a Self-Assembled Organic Molecular Template. *J. Phys. Chem. Lett.* **2011**, *2*, 1639–1645.
43. Auwärter, W.; Weber-Bargioni, A.; Brink, S.; Riemann, A.; Schiffrin, A.; Ruben, M.; Barth, J. V. Controlled Metalation of Self-Assembled Porphyrin Nanoarrays in Two Dimensions. *ChemPhysChem* **2007**, *8*, 250–254.
44. Auwärter, W.; Klappenberger, F.; Weber-Bargioni, A.; Schiffrin, A.; Strunskus, T.; Wöll, C.; Pennec, Y.; Riemann, A.; Barth, J. V. Conformational Adaptation and Selective Adatom Capturing of Tetrapyridyl-Porphyrin Molecules on a Copper (111) Surface. *J. Am. Chem. Soc.* **2007**, *129*, 11279–11285.
45. Klappenberger, F.; Weber-Bargioni, A.; Auwärter, W.; Marschall, M.; Schiffrin, A.; Barth, J. V. Temperature Dependence of Conformation, Chemical State, and Metal-Directed Assembly of Tetrapyridyl-Porphyrin on Cu(111). *J. Chem. Phys.* **2008**, *129*, 214702.
46. Classen, T.; Fratesi, G.; Costantini, G.; Fabris, S.; Stadler, F. L.; Kim, C.; De Gironcoli, S.; Baroni, S.; Kern, K. Templated Growth of Metal−Organic Coordination Chains at Surfaces. *Angew. Chem., Int. Ed.* **2005**, *44*, 6142–6145.
47. Ditze, S.; Stark, M.; Buchner, F.; Aichert, A.; Jux, N.; Luckas, N.; Görling, A.; Hieringer, W.; Hornegger, J.; Steinrück, H.-P.; *et al.* On the Energetics of Conformational Switching of Molecules at and Close to Room Temperature. *J. Am. Chem. Soc.* **2014**, *136*, 1609–1616.
48. Hieringer, W.; Flechtner, K.; Kretschmann, A.; Seufert, K.; Auwärter, W.; Barth, J. V.; Görling, A.; Steinrück, H.-P.; Gottfried, J. M. The Surface Trans Effect: Influence of Axial Ligands on the Surface Chemical Bonds of Adsorbed Metalloporphyrins. *J. Am. Chem. Soc.* **2011**, *133*, 6206–6222.
49. Fano, U. Effects of Configuration Interaction on Intensities and Phase Shifts. *Phys. Rev.* **1961**, *124*, 1866–1878.
50. Li, J.; Schneider, W.-D.; Berndt, R.; Delley, B. Kondo Scattering Observed at a Single Magnetic Impurity. *Phys. Rev. Lett.* **1998**, *88*, 2893–2896.
51. Madhavan, V.; Chen, W.; Jamneala, T.; Crommie, M. F.; Wingreen, N. S. Tunneling into a Single Magnetic Atom: Spectroscopic Evidence of the Kondo Resonance. *Science* **1998**, *280*, 567–569.

52. Manoharan, H. C.; Lutz, C. P.; Eigler, D. M. Quantum Mirages Formed by Coherent Projection of Electronic Structure. *Nature* **2000**, *403*, 512–515.
53. Fernández-Torrente, I.; Franke, K. J.; Pascual, J. I. Vibrational Kondo Effect in Pure Organic Charge-Transfer Assemblies. *Phys. Rev. Lett.* **2008**, *101*, 217203.
54. Müllegger, S.; Rashidi, M.; Fattinger, M.; Koch, R. Surface-Supported Hydrocarbon π Radicals Show Kondo Behavior. *J. Phys. Chem. C* **2013**, *117*, 5718–5721.
55. Zhao, A.; Li, Q.; Chen, L.; Xiang, H.; Wang, W.; Pan, S.; Wang, B.; Xiao, X.; Yang, J.; Hou, J. G.; *et al.* Controlling the Kondo Effect of an Adsorbed Magnetic Ion through Its Chemical Bonding. *Science* **2005**, *309*, 1542–1544.
56. Iancu, V.; Deshpande, A.; Hla, S. W. Manipulation of the Kondo Effect *via* Two-Dimensional Molecular Assembly. *Phys. Rev. Lett.* **2006**, *97*, 266603.
57. Iancu, V.; Deshpande, A.; Hla, S. W. Manipulating Kondo Temperature *via* Single Molecule Switching. *Nano Lett.* **2006**, *6*, 820–823.
58. Gao, L.; Ji, W.; Hu, Y. B.; Cheng, Z. H.; Deng, Z. T.; Liu, Q.; Jiang, N.; Lin, X.; Guo, W.; Du, S. X.; *et al.* Site-Specific Kondo Effect at Ambient Temperatures in Iron-Based Molecules. *Phys. Rev. Lett.* **2007**, *99*, 106402.
59. Tsukahara, N.; Shiraki, S.; Itou, S.; Ohta, N.; Takagi, N.; Kawai, M. Evolution of Kondo Resonance from a Single Impurity Molecule to the Two-Dimensional Lattice. *Phys. Rev. Lett.* **2011**, *106*, 187201.
60. Minamitani, E.; Tsukahara, N.; Matsunaka, D.; Kim, Y.; Takagi, N.; Kawai, M. Symmetry-Driven Novel Kondo Effect in a Molecule. *Phys. Rev. Lett.* **2012**, *109*, 086602.
61. Heinrich, B. W.; Ahmadi, G.; Müller, V. L.; Braun, L.; Pascual, J. I.; Franke, K. J. Change of the Magnetic Coupling of a Metal−Organic Complex with the Substrate by a Stepwise Ligand Reaction. *Nano Lett.* **2013**, *13*, 4840–4843.
62. Néel, N.; Kröger, J.; Limot, L.; Palotas, K.; Hofer, W. A.; Berndt, R. Conductance and Kondo Effect in a Controlled Single-Atom Contact. *Phys. Rev. Lett.* **2007**, *98*, 016801.
63. Vitali, L.; Ohmann, R.; Stepanow, S.; Gambardella, P.; Tao, K.; Huang, R.; Stepanyuk, V. S.; Bruno, P.; Kern, K. Kondo Effect in Single Atom Contacts: The Importance of the Atomic Geometry. *Phys. Rev. Lett.* **2008**, *101*, 216802.
64. Néel, N.; Kröger, J.; Berndt, R. Kondo Effect of a Co Atom on Cu(111) in Contact with an Iron Tip. *Phys. Rev. B* **2010**, *82*, 233401.
65. Choi, D.-J.; Rastei, M. V.; Simon, P.; Limot, L. Conductance-Driven Change of the Kondo Effect in a Single Cobalt Atom. *Phys. Rev. Lett.* **2012**, *108*, 266803.